S E S 2 0 2 5

Twenty-first International Scientific Conference SPACE, ECOLOGY, SAFETY 21 – 25 October 2025, Sofia, Bulgaria

SPACE RADIATION INVESTIGATIONS WITH LYULIN-TYPE INSTRUMENTS IN THE PERIOD 1989–2022

Tsvetan Dachev¹, Borislav Tomov¹, Yuriy Matviichuk¹, Mityo Mitev¹, Malina Yordanova¹, Jordanka Semkova¹, Victor Benghin², Viacheslav Shurshakov², Donat-Peter Haeder³, Gerda Horneck⁴, Guenther Reitz⁴, Frantisek Spurni⁵, Ondrej Ploc⁵, William Tobiska⁶, Benjamin Hogan⁶, Brad Gersey⁶

¹Space Research and Technology Institute – Bulgarian Academy of Sciences
²State Scientific Center of Russian Federation, Institute of Biomedical Problems, Moscow, Russia
³Department of Biology, Friedrich-Alexander Universität Erlangen-Nürnberg, Möhrendorf, Germany
⁴DLR, Institute of Aerospace Medicine, Köln, Germany
⁵Nuclear Physics Institute of the Czech Academy of Sciences, Prague, Czech Republic
⁶Space Weather Division, Space Environment Technologies, Los Angeles, CA, USA
e-mail: tdachev59@gmail.com

Keywords: Liulin spectrometer-dosimeters, space radiation, galactic cosmic rays, radiation belts

Abstract: The first Liulin-type spectrometers-dosimeter was developed in connection with the scientific program of the second Bulgarian cosmonaut Alexander Alexandrov in 1986–1988. It worked on the Mir space station from 1988 until 1994.

Until 2022, 35 Liulin-type spectrometers-dosimeters were developed. Twenty one of them were tested and qualified for operation in space. Three of these twenty dosimeters did not reach the planned orbits around the Earth and Mars due to technical problems with the carriers. The scientific programs of 12 of these 20 Liulins were to measure the variations of the flux and dose rate of cosmic radiation on satellites, space stations in orbit around the Earth. Two instruments conducted measurements in interplanetary space and around the Moon and Mars: The RADOM instrument operated on the track to Moon and in circular orbit around the Moon. The Liulin-MO dosimeter is active since 2016 on the track and in a 400 km circular orbit around Mars. The scientific objectives of eight spectrometers were to support biological and chemical experiments in space with up-to-date information on the history of dose accumulation. This paper presents the most interesting scientific results on the dose and flux of cosmic radiation obtained recently.

ИЗСЛЕДВАНЕ НА КОСМИЧЕСКАТА РАДИАЦИЯ С ПРИБОРИ ОТ ТИПА ЛЮЛИН В ПЕРИОДА 1989–2022 Г.

Цветан Дачев¹, Борислав Томов¹, Пламен Димитров¹, Юрий Матвийчук¹, Митьо Митев¹, Малина Йорданова¹, Йорданка Семкова¹, Виктор Бенгин², Вячеслав Шуршаков², Донат-Петер Хедар³, Герда Хорнек⁴, Гюнтер Райтц⁴, Франтишек Спурни⁵, Ондреж Плоц⁵, Уйлям Тобиска⁶, Бенжамин Хоган⁶, Брад Герси⁶

¹Институт за космически изследвания и технологии (ИКИТ) – Българска академия на науките ²Държавен научен център на Руската федерация, Институт по биомедицински проблеми, Москва, Русия

³Катедра по биология, Университет "Фридрих-Александър" Ерланген-Нюрнберг, Мьорендорф, Германия ⁴Институт по аерокосмическа медицина, Кьолн, Германия

⁵Институт по ядрена физика на Чешката академия на науките, Прага, Чехия ⁶Отдел за космическо време, Технологии за космическа среда, Лос Анджелис, Калифорния, САЩ e-mail: tdachev59 @gmail.com

Ключови думи: Спектрометри-дозиметри "Люлин", космическа радиация, галактически космически лъчи, радиационни пояси

Резюме: Първият спектрометр-дозиметър от типа Люлин е разработен във връзка с научната програма на втория български космонавт Александър Александров през 1986–1988 г. Той работи на орбиталната станция "Мир" в периода 1988–1994 г.

До 2022 г. са разработени 35 дозиметъра от типа Люлин, 21 от които са тествани и квалифицирани за работа в космоса. Три от тези двадесет дозиметъра не достигат планираните орбити около Земята и Марс поради технически проблеми с носителите.

Научните програми на 12 от 20-те Люлини са измерване на вариациите на потока и мощността на дозата от космическа радиация на спътници и станции в орбити около Земята. Два от 12-те спектрометъра провеждат измервания в междупланетното пространство около Луната и Марс: Приборът RADOM работи по трасето и в орбита около Луната в периода 2008–2009 г. Приборът Люлин-МО е активен от 2016 г. досега по трасето до Марс и на 400 km кръгова орбита около Марс.

Научните програми на 8 от Люлините подкрепят биологични и химични експерименти в космоса с актуална информация за историята на натрупване на дозата космическа радиация. Тази статия представя най-интересни научни резултата за дозата и потока от космическа радиация, получени наскоро.

Introduction

Cosmic ionizing radiation is one of the main risks to human health in space. Galactic cosmic rays (GCRs) are the dominant radiation source in the space environment. GCRs are not rays at all, but charged particles that are generated by sources outside the Solar System such as neutron stars and supernovae. GCRs have the highest penetrating power among the main types of ionizing radiation. The energy of the particles (87% protons, 12% helium nuclei and 1% heavier ions) in GCRs ranges from a few tens to 10¹² MeV per nucleon [1].

Another source of radiation in space are the solar energetic particles (SEPs) generated during solar eruptions. They are accelerated in sudden sporadic eruptions from the Sun's chromosphere and can accumulate even lethal doses for crews in interplanetary space and on the surfaces of the Moon and Mars. SEPs consist mainly of protons and a small percentage of helium and heavier ions. The maximum energy that SEPs reach is up to several GeV [2].

In the radiation belts, high-energy charged particles, trapped by the Earth's geomagnetic field, are found. The inner radiation belt (IRB) is located at heights between 1.1 and 2 Earth radii and consists of electrons with energies up to 10 MeV and protons with energies up to 700 MeV. The high doses of radiation in it limit the maximum altitude at which manned space stations could be located to the lower limit of the IRB, which is about 600 km from the Earth's surface.

The outer radiation belt (ORB) starts at about four Earth radii and extends to about 9–10 Earth radii in the direction of the Sun. It consists mainly of electrons with energies below 10 MeV that cannot penetrate the walls of the spacecraft, but could deliver large additional doses to cosmonauts and astronauts during work outside the station [3].

Theoretical calculations show that cosmic radiation doses during a flight to Mars could easily exceed the maximum permissible limits [4]. Therefore, experimental measurements of cosmic radiation doses during unmanned missions are of great importance for future planning of flights in interplanetary space and on the surface of the Moon and Mars.

Instruments Description

The first Liulin-type spectrometers-dosimeter was developed in connection with the scientific program of the second Bulgarian cosmonaut Alexander Alexandrov in 1986–1988. It worked on the Mir space station from 1988 until 1994.

Since 1989, Space Research and Technology Institute (SRTI-BAS), in an international cooperation with scientists from Russia, Germany, Japan, Czech Republic, Italy, Norway, Switzerland, Belgium, USA and India, etc., worked at mountain peaks, flew in space and on stratospheric balloons, rockets and aircraft with more than 35 Liulin-type spectrometers-dosimeter [5], (http://www.space.bas.bg/SollarTerrestialPhysics/files/Poster-IKIT-BAN-2019%20SZF.pdf). 21 of these Liulin-type spectrometers-dosimeters were developed, tested and qualified for operation in space.

The latest application of Liulin device are:

- (a) The flight of Liulin-SET instrument on Japanese external module of THE International Space station (ISS) in March-December 2022 [6];
- (b) The flight of the first commercial mission into suborbital space with the SpaceShipTwo spacecraft of Virgin Galactic Company (Virgin Galactic launches first commercial spaceflight (spacedaily.com). The flight took place on June 29th, 2023 at 08:00 a.m. MT or 03:00 p.m. GMT from Spaceport America in New Mexico, USA [7].

Liulin spectrometers contain one silicon-PIN diode of Hamamatsu S2744-08 type (2 cm² area and 0.3 mm thickness), one ultra-low noise charge-sensitive preamplifier of AMPTEK A225F type, and 2 microcontrollers (Please look a Fig. 2 of [5]).

The doses (deposited energies in the detector) are determined by a pulse height analysis technique then passed to a discriminator. According to AMPTEK A225 specifications, the pulse amplitudes A [V] are proportional by a factor of 240 mV/MeV to the energy loss in the detector and respectively to the dose. This is the key feature of the AMPTEK A225 preamplifier, which directly transfers the pulse amplitude, measured in volts by the spectrometer to dose and dose rate.

The amplitudes of all signals from the income particles and quanta are transformed into digital signals by ADC converter and are sorted into 256 channels by a multichannel analyzer. For every exposure interval, a single 256 energy deposited spectrum is collected.

Two microcontrollers, through specially developed firmware, manage the unit. Liulin communicates with a personal computer by a universal serial bus (USB) signal.

Two Liulin type spectrometer-dosimeters, Liulin-5 and Liulin-MO, are built as two detector telescopes [8, 9] under the scientific leadership of Prof. Dr.S. Jordanka Semkova.

The following method for calculations of the dose is used [5]: The dose D [Gy] by definition is one Joule of energy deposited in 1 kg of a mater or:

(1) $D = K.Sum(EL_1*i)_{ET}/MD,$

where MD is the mass of the detector in [kg] and EL_i is the energy loss in Joules in channel i. The energy loss in channel i is proportional to the number of events A_i in it multiplied by i. K is a coefficient.

Scientific Results

Radiation Sources Selection Procedures

The first selection procedure is described by Dachev et al. [10]. More sophisticated selection procedure is also published by Dachev et al. 2017 [11].

The following three primary radiation sources were expected and recognized by the data selection procedures designed for the Liulin instruments: (i) globally distributed primary GCR particles and their secondary products; (ii) protons in the South Atlantic Anomaly (SAA) region of the IRB; (iii) relativistic electrons and/or bremsstrahlung in the high latitudes of the ISS orbit where the ORB is situated.

Global Distribution of the Radiation Sources

Fig. 1 presents the averaged contour view of the global map of the flux data obtained with four Liulin type instruments as follows: LIULIN inside MIR space station (MIR SS) in March 1991; Liulin E94 inside Russian segment of the ISS in May 2001; R3DR2 outside the Russian segment of the ISS in June 2015 and Liulin-SET outside the Japanize Experimental Module of the ISS in October 2022.

Figure 1 illustrates: 1) the positions of the primary radiation sources and 2) explores the secular movement of the center of SAA region of the Inner Radiation belt toward North-West direction.

The first panel of Fig. 1 (a, In ("In" means inside the MIR SS)) shows the two flux rates sources: a) the GCR particles and their secondary and b) the IRB energetic protons, trapped in the Earth magnetic field in the region of the SAA. The smallest GCR flux rates (less than 0.13 cm⁻² s⁻¹) are observed in the low latitude region, while the largest (up to 25-µGy h⁻¹) are observed in the high latitude regions. Similar is the distributions of the fluxes observed with Liulin-E094 instrument inside the American Laboratory module of the ISS seen in the second panel (Fig. 1 b, In).

The bottom panels of the figure present data registered while R3DR2 and Liulin-SET instruments are outside the ISS. The significantly smaller shielding allows energetic electrons from the ORB to reach the detector. New patches in the high latitude of the global map appear [10] in Fig. (1c, Out). These patches are labeled with "ORB". They appears in both hemispheres. The ORB patch in Southern hemisphere at longitudes 0° –35° East longitude is created during magnetic storm events. The presence of energetic protons during Solar Energetic Particle Events (SEP), is also seen in the high latitudes of the global map [12].

Secular Movement of the Center of South Atlantic Anomaly

Due to the secular evolution of the geomagnetic field, the location of the SAA slowly changes.

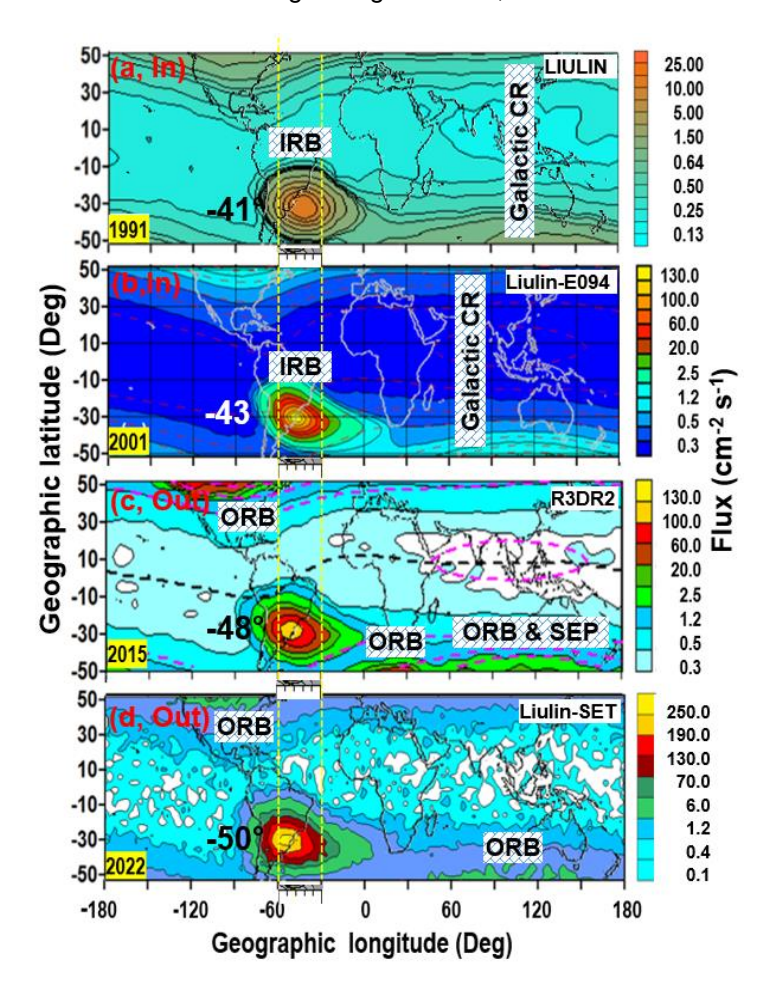


Fig. 1. Averaged contour view of the global map of the flux data obtained with four Liulin type instruments on MIR SS and ISS in the period March 1991 – October 2022

The SAA center shows a westward drift. However, the drift speed is different: the location of minimum of geomagnetic field drifts 0.18° per year; while the particle flux maximum drifts 0.3° per year. The numerous observations of particle flux show that the center of South Atlantic Anomaly drifts westward, while the meridional movements are not consistent [12].

Two vertical, dotted, yellow lines are drawn in all four panels of Fig. 1. Their positions are at -30° and -60° West longitude. Between these lines a better resolution scale of X-axis with 6-degree step is drawn. Using it, the West longitude of the SAA is found at every panel. The results are shown on the left side from -60° West longitude. The values there are from top to bottom -41°, -43°,-48° and -50°. The calculated difference is 9° for 31 years from 1991 and 2022. The yearly drift rate is 9/31=0.29° per year. This value is very close to the overviewed in [13].

Geomagnetic Storm Effects Observed with R3DR2 Instrument outside the ISS in 2014-2016

Figure 2 presents two 3-dimensional L value versus time plots of the average ORB and IRB flux rates in cm⁻² s⁻¹ against the color bar in the middle-right part of the figure between October 24, 2014 and December 24, 2015.

The upper panel of the figure presents the ORB relativistic electrons more than 0.835 MeV flux variations, while the lower panel the IRB more than 19.5 MeV proton flux variations. The plotted values in the 2 panels, are the average observed per day per the bin flux values. The bins with size of 0.02 L value units are organized in a 442 daily vertical bars, which are plotted against the date form the two 3 dimensional plots.

In the upper panel with heavy white line are plotted the daily Dst index variations (http://wdc.kugi.kyoto-u.ac.jp/index.html). Along the bottom-right vertical axes of the lower panel with heavy white line is plotted the daily average altitude of the station, which was obtained for the locations of the daily average IRB flux.

The ISS average flux bins cover the whole L values range from 1 to 6 in the Southern hemisphere, while in the Northern hemisphere the flux data bins are extended only up to L=4.7, because the Earth magnetic field hemisphere asymmetries. This explains the borderline seen in Fig. 4a at L=4.7 and the smaller population of the bins in the L range between 4.7 and 6.

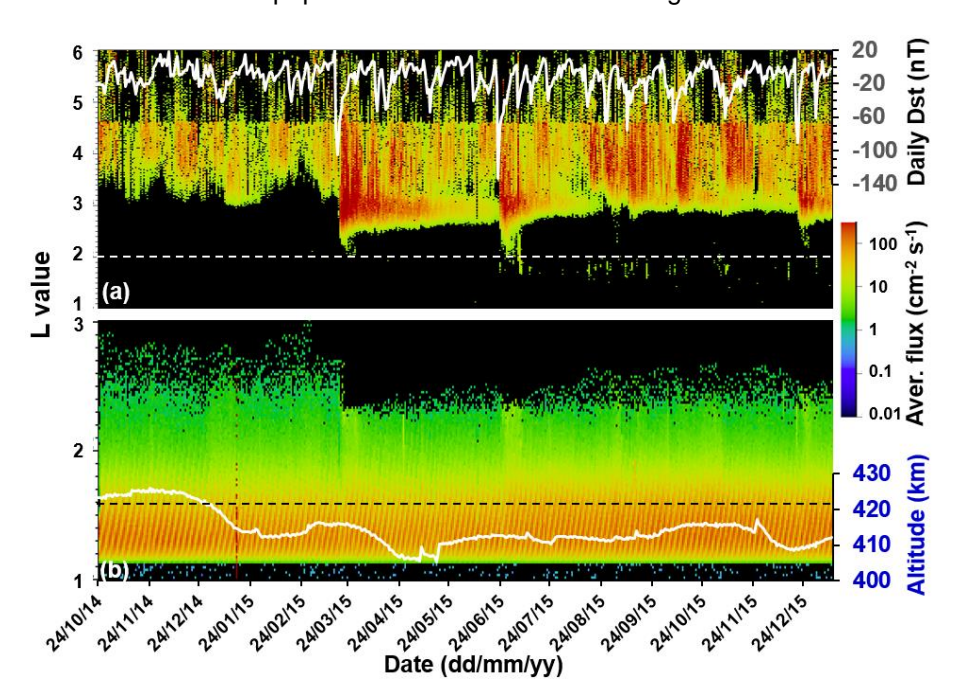


Fig. 2. The 3-dimensional L value versus time plot presents the average observed in the bin flux rate in cm⁻² s⁻¹ against the color bar in the middle-right part of the figure

Following peculiarities and geomagnetic activity effects are seen in the Fig. 2 panels:

- Fig. 2a:
- The measured by the R3DR2 instrument ORB flux rates in the range 3.3–11,814 cm⁻² s⁻¹ with average value of 85 cm⁻² s⁻¹ dominate the IRB rates, which are in the range 0.15–304 cm⁻² s⁻¹ with an average value of 35.9 cm⁻² s⁻¹;
- Two periods are clearly seen. In the relatively "quiet" period between October 24, 2014 and the middle of March 2015, the ORB flux time and space variations are relatively small and varied in the interval between 1 and 50–60 cm⁻² s⁻¹. In this period, the equatorward boundary of the ORB vary in the interval of L values between 3 and 4. The ORB relativistic electrons equatorward boundary never penetrate at L values below 3;
- The penetration of relativistic electrons down to L values below 2 and the strong temporary enhancements of the maximal flux, seen in the 3D plot of Fig. 2a, usually take place in the main phase of the magnetic storm, when the negative value of Dst is large. (In Fig. 2 the daily Dst index variations (http://wdc.kugi.kyoto-u.ac.jp/index.html) in nT are depicted as white line against the upper-right vertical axes.) Later, during the recovery phase of the magnetic storm, the ORB equatorial boundary moved from about L = 2.4 back to L = 3.0. These features were repeatedly registered during the storms in March, June and December 2015. Most of the time the ORB was with single maximum distribution in the L profile but after the storms in March and June 2015, periods with two maxima were registered. Although not well visible, the best example of two maxima L distribution profile, seen in Fig. 2a, is the period between May 20 and June 20, 2015. The two maxima L distribution profiles were detected mainly in the southern hemisphere and are similar to the "third" Van Allen radiation belt phenomena, recently explained by Mann et al. [14];
- Similarly to Claudepierre et al. [15] and Turner et al. [16], we have recorded penetration of the relativistic electrons below L = 2.5 on 18 March 2015. In the period March 18–28 2015, the lower boundary of L = 2 was reached. After that period, the relativistic electrons at low L disappeared on March 28th 2015. The storm on June 25th generated again fluxes of the ORB relativistic electrons at L values below 2 and they are clearly seen in Fig. 2a. The ORB enhancement on 4th July 2015 emphasized them again but at this case the minimal L values reached was L = 1.6. Almost all disturbances in the Dst from July 11th, 2015 until December 2015 generated a new portion of relativistic electrons in the range of L values between 1.6 and 2. They existed for 1–2 days and disappeared until the next Dst disturbance.

Fig. 2b:

- The flux rates in the SAA maximum at L values between 1.2 and 1.4 strongly depend on the altitude of the station, presented with heavy white line in Fig 2b against the lower-right axes in the figure. The maximum flux values in the period 24 October–24 December 2014 is connected with the highest altitudes of the station above 420 km in this period. The wide maximum, between June 2015 and till the end of the graph, is generated not only by the relative high altitudes but also by the smaller solar activity, which lowered the neutral atmosphere density and decrease the sink of the IRB energetic protons;
- The "quiet" and disturbed periods in Fig. 2b are also clearly seen. During the "quiet" period the poleward boundary of the inner radiation belt extends up to L = 3. The first strong magnetic storm on 17th of March 2015 decreases the IRB poleward boundary down to L = 2.3. During the months April, May and partly June the boundary slowly moves back to level of L = 2.5. Next strong storm in June push it again down to level of L = 2.3. In the period between July and December the boundary extends back to value of L = 2.7. Next relatively smaller storm on 21st of December bring it down to L = 2.5. Very scrupulously comparison between the ORB equatorward and IRB poleward boundaries shows that they move simultaneously in same direction with different L value rate;
- During the main phases of the storms on 17 March and 25 June 2015 is seen a decrease of the IRB fluxes in the whole L value range;
- During the recovery phases reverse process of enhancement of the IRB fluxes also in the whole L value range takes place.

Long-term Solar Modulation of Galactic Cosmic Rays (GCR) Distribution

The long-term solar modulation of GCR is observed experimentally and already published for the period 1991–2019 [17]. On Figure 3 we update these results by data from the Liulin-SET instrument from September 2022 [6].

The total number of measurements exceeds 12,000,000. Most of them are available free from the "Unified Web-based Database with Liulin-type Instruments" at http://esa-pro.space.bas.bg/database. As the paper is focused on the L values between 4 and 6.2, only 613,397 measurements are used for this study.

Data collected in 15 space experiments, covering three decades and almost three solar cycles were obtained using the same type of devices, which makes the results comparable.

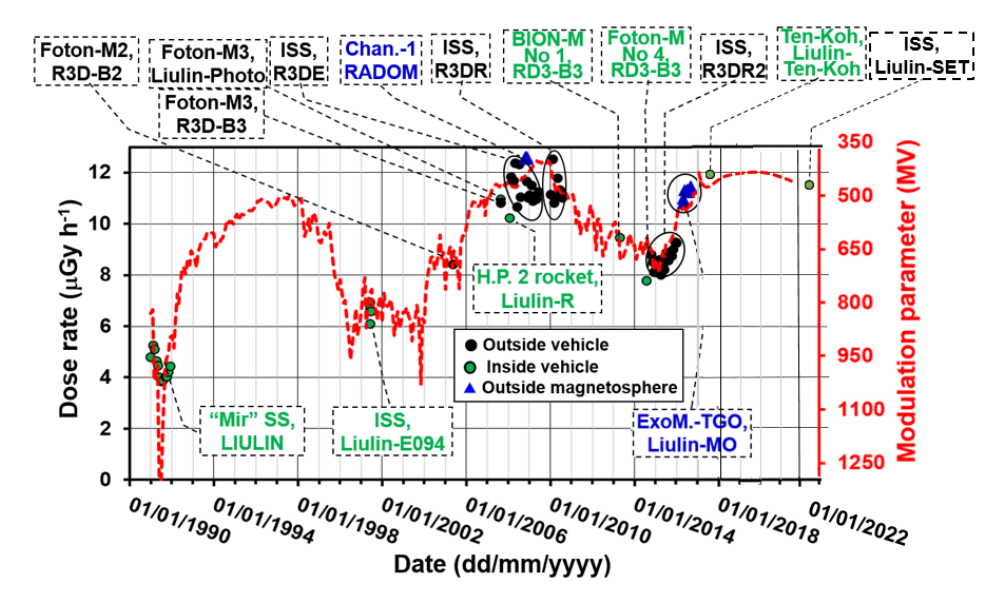


Fig. 3. Long-term variations of the averaged dose rates observed in the L range between 4 and 6.2 (black and dark-green points) or outside the magnetosphere (blue triangles) during 15 experiments between 1989 and 2022. The Liulin data are compared with the monthly values of the modulation parameter (red line) in MV.

Conclusions

The most important advantage of this study is that electronically identical Liulin type instruments obtain the data sets. These experimentally gotten flux and dose rate data could be used for modelling of the space radiation risks to humans in the near Earth radiation environment.

Acknowledgements:

Most of the data, used in this paper, are part of the "Unified Web-Based Database with Liulin-type Instruments", which are available online, free of charge at the following URL: https://esa-pro.space.bas.bg/database.

References:

- 1. Simpson J.A., in: Shapiro M.M. (Ed.) Composition and origin of cosmic rays, NATO ASI Series C: Mathematical and Physical Sciences. Vol. 107, Reidel, Dordrecht, 1983
- Anastasiadis, A., Lario, D., Papaioannou, A., Kouloumvakos, A. and Vourlidas, A., Solar energetic particles in the inner heliosphere: status and open questions. *Philosophical Transactions of the Royal Society A*, 377(2148), p. 20180100, 2019. Dachev, T.P., Relativistic Electron Precipitation Bands in the Outside Radiation Environment of the International Space Station, Journal of Atmospheric and Solar-Terrestrial Physics, 177, 247-256, 2018, https://doi.org/10.1016/j.jastp.2017.11.008
- 3. Häder, D.P., et al., R3D-B2 Measurement of ionizing and solar radiation in open space in the BIOPAN 5 facility outside the FOTON M2 satellite, Adv. Space Res. 43, 1200–1211, 2009. doi:10.1016/j.asr.2009.01.021
- Semkova, J., et al., Charged particles radiation measurements with Liulin-MO dosimeter of FREND instrument aboard ExoMars Trace Gas Orbiter during the transit and in high elliptic Mars orbit. Icarus, Volume 303, 15 March 2018, Pages 53–66, 2018. https://doi.org/10.1016/j.icarus.2017.12.034
- 5. Dachev, T. P., et al., Overview of the Liulin type instruments for space radiation measurement and their scientific results, Life Sciences in Space Research, 4, 92–114, 2015. http://dx.doi.org/10.1016/j.lssr.2015.01.005
- Tobiska, K., et al., International space station radiation field measurements by Liulin-SET spectrometer of ARMAS flight module 9 in 2022, 20th Proceedings of the Twentieth International Scientific Conference "SPACE, ECOLOGY, SAFETY" – SES 2024, pp. 16–22, October, 2024, Sofia, Bulgaria
- 7. Dachev, T., Carlucci, P., Cairo, F., Tomov, B., Matviichuk, Y., Dimitrov, P., Mitev, M., Jordanova, M. and Paciucci, L., 2025. Space radiation measured during first-ever commercial suborbital mission on Virgin Galactic SpaceShipTwo Unity on 29 June 2023. *Life Sciences in Space Research*, *44*, pp. 126-133, https://doi.org/10.1016/j.lssr.2024.09.003
- 8. Semkova, J., R. Koleva, St. Maltchev, G. Todorova, Ts. Dachev, V. Benghin, V. Shurshakov, V. Petrov, Calibration results of Liulin-5 charged particle telescope obtained in ICCHIBAN-7 experiment. New instrumentation for radiation monitoring on interplanetary missions, presented at the 11th Workshop on Radiation Monitoring for the International Space Station (WRMISS) held in Oxford, UK, September 6–8, 2006. chrome- https://wrmiss.org/workshops/eleventh/Semkova.pdf
- Semkova, J., Koleva, R., Benghin, V., Dachev, T., Matviichuk, Y., Tomov, B., Krastev, K., Maltchev, S., Dimitrov, P., Mitrofanov, I. and Malahov, A., 2018. Charged particles radiation measurements with Liulin-MO dosimeter of FREND instrument aboard ExoMars Trace Gas Orbiter during the transit and in high elliptic Mars orbit. *Icarus, Volume 303, 15 March 2018, Pages 53–66,* https://doi.org/10.1016/j.icarus.2017.12.034
- Dachev, Ts., G. Horneck, D.-P. Häder, M. Lebert, P. Richter, M. Schuster, R. Demets, 2012b. Time profile of cosmic radiation exposure during the EXPOSE-E mission: the R3D instrument, Journal of Astrobiology, 12, 5, 403-411, http://dx.doi.org/10.1089/ast.2011.0759
- Dachev, T. P., Bankov, N. G., Tomov, B. T., Matviichuk, Y. N., Dimitrov, P. G., Häder, D. P. & Horneck, G. Overview of the ISS radiation environment observed during the ESA EXPOSE-R2 mission in 2014–2016. Space Weather, 15, 1475–1489, 2017. https://doi.org/10.1002/2016SW001580
- 12. Dachev, T.P., B. T. Tomov, Yu. N. Matviichuk, Pl. G. Dimitrov, N.G. Bankov, High dose rates obtained outside ISS in June 2015 during SEP event, Life Sciences in Space Research, 9, 84–92, 2016, http://dx.doi.org/10.1016/j.lssr.2016.03.004
- 13. Ye, Y., Zou, H., Zong, Q., Chen, H., Wang, Y., Yu, X. and Shi, W. The secular variation of the center of geomagnetic South Atlantic Anomaly and its effect on the distribution of inner radiation belt particles. Space Weather, 15(11), pp. 1548–1558, 2017
- Mann, I.R., Ozeke, L.G., Murphy, K.R., Claudepierre, S.G., Turner, D.L., Baker, D.N., Rae, I.J., Kale, A., Milling, D.K., Boyd, A.J. and Spence, H.E., Explaining the dynamics of the ultra-relativistic third Van Allen radiation belt. Nature Physics, 12(10), pp. 978–983, 2016
- Claudepierre, S.G., O'Brien, T.P., Fennell, J.F., Blake, J.B., Clemmons, J.H., Looper, M.D., Mazur, J.E., Roeder, J.L., Turner, D.L., Reeves, G.D. and Spence, H.E., The hidden dynamics of relativistic electrons (0.7–1.5 MeV) in the inner zone and slot region. Journal of Geophysical Research: Space Physics, 122(3), pp. 3127–3144, 2017
- 16. Turner, D.L., et al., Investigating the source of near-relativistic and relativistic electrons in Earth's inner radiation belt. J. Geophys. Res. Space Phys. 122, 695–710. 2017
- 17. Dachev TP, Tomov BT, Matviichuk YN, Dimitrov PG, Semkova JV, Koleva RT, Jordanova MM, Bankov NG, Shurshakov VA, Benghin VV. Solar modulation of the GCR flux and dose rate, observed in space between 1991 and 2019. Life Sciences in Space Research. Aug 1; 26:114–24, 2020.